JACS
JOURNAL OF THE AMERICAN CHEMICAL SOCIETY
Communication
pubs.acs.org/JACS

Slow-Reduction Synthesis of a Thiolate-Protected One-Dimensional Gold Cluster Showing an Intense Near-Infrared Absorption

Shinjiro Takano,[†] Seiji Yamazoe,[†,‡] Kiichirou Koyasu,[†,‡] and Tatsuya Tsukuda*[,†,‡]

[†]Department of Chemistry, School of Science, The University of Tokyo, 7-3-1 Hongo, Bunkyo-ku, Tokyo 113-0033, Japan
[‡]Elements Strategy Initiative for Catalysis and Batteries (ESICB), Kyoto University, Katsura, Kyoto 615-8520, Japan

Supporting Information

ABSTRACT: Slow reduction of Au ions in the presence of 4-(2-mercaptoethyl)benzoic acid (4-MEBA) gave $Au_{76}(4\text{-MEBA})_{44}$ clusters that exhibited a strong (3×10^5 M^{-1} cm^{-1}) near-infrared absorption band at 1340 nm. Powder X-ray diffraction studies indicated that the Au core has a one-dimensional fcc structure that is elongated along the {100} direction.

Gold nanostructures exhibit unique optical properties that depend on their dimensions and morphology. It is well established that isotropic gold nanoparticles (AuNPs) with diameters of >2 nm exhibit localized surface plasmon (LSP) bands centered at ~520 nm.[1−3] If the diameter of the AuNPs is less than 2 nm, the LSP band disappears and the clusters begin to evolve an optical onset, corresponding to electronic transitions between the HOMO and LUMO.[4−6] Such small Au clusters show distinct peaks and humps in the UV−vis region, reflecting the presence of discrete electronic energy levels. As a result of recent developments in methods for atomically precise synthesis of thiolate (SR)-protected gold clusters (Au:SR), the evolution of their optical spectra as a function of size has been revealed.[6−9]

Gold nanorods with diameters of >10 nm show two distinct LSP bands associated with longitudinal and transverse modes, respectively.[1−3] Optical absorption spectra of ultrathin Au nanowires and nanorods (Au UNWs and Au UNRs) with diameters of ~1.6 nm have recently been reported.[10] These do not show an LSP band at ~520 nm because of their very low diameters, but they do show a strong LSP band in the near infrared (NIR)−IR region. Theoretical studies predict that linear assemblies of icosahedral Au_{13} units and ultrasmall Au nanorods should exhibit distinct absorption peaks in the NIR region due to photoexcitation of an electron confined in a one-dimensional box or a longitudinal mode of LSP.[11−16] Here, we report the synthesis of ultrasmall one-dimensional Au clusters that display an intense absorption band in the NIR region.

Details of the slow-reduction synthesis are presented in the Supporting Information.[17] Briefly, 4-(2-mercaptoethyl)benzoic acid (4-MEBA) was mixed with $HAuCl_4$ in aqueous ethanolic solution. The pH was adjusted to >12 by adding aqueous NaOH, and then aqueous $NaBH_4$ was added to initiate reduction. The reduction proceeded much more slowly under the basic conditions than it would have under acidic conditions. The reaction was stopped after 96 h when the spectral profile ceased to change appreciably (Figure S1).[17] The crude products collected by centrifugation were purified by gel filtration. A small fraction having the shortest retention time (yield ≈ 2%, Au basis) was used as sample **1**. The residue of the gel filtration showed exponential-like, featureless optical spectrum typically observed for Au clusters with a diameter of <2 nm (red curve in Figure S1) and did not contain ubiquitous clusters, such as $Au_{25}(SR)_{18}$ and $Au_{38}(SR)_{24}$.[17]

A dispersion of sample **1** in water appeared greenish (Figure 1a, inset). Figure 1a shows the UV−vis−NIR spectra of **1** measured at room temperature. The spectrum of **1** dispersed in water (red curve) shows small peaks at 400, 580, and 680 nm, indicating the quantized electronic structure. The spectrum of wider wavelength region (300−2000 nm) was recorded after dry up of **1** on a CaF_2 substrate to avoid interference from water (green curve). Interestingly, an intense band was observed at 1350 nm. The peaks in the UV−vis region are slightly obscured in the film spectrum, posing a concern that **1** was degraded in the solid form. However, the peaked structures in the UV−vis region became clearer by lowering the temperature to 20 K (blue curve) and were recovered after redispersion of the film in water. These observations indicate that the peak broadening is not due to the irreversible degradation of **1**. To measure the NIR spectra in

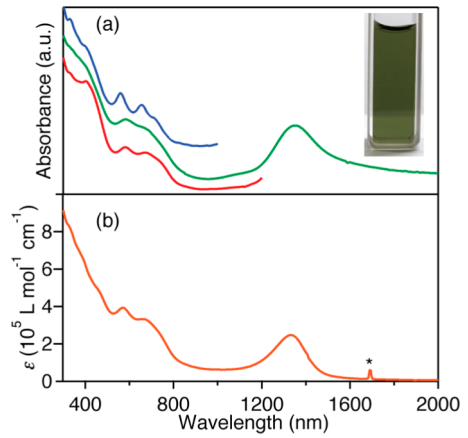

Figure 1. (a) UV−vis−NIR absorption spectra of **1** in water (red), as a thin film at room temperature (green) and at 20 K (blue). The blue curve is offset vertically for clarity. The inset photograph shows a dispersion of **1** in water. (b) UV−vis−NIR absorption spectrum of **2** dispersed in $CHCl_3$. The asterisk indicates the absorption of the $CHCl_3$ solvent.

Received: March 28, 2015
Published: May 28, 2015

DOI: 10.1021/jacs.5b03251
J. Am. Chem. Soc. 2015, 137, 7027−7030

$CHCl_3$, which is transparent in this region, the 4-MEBA ligands of **1** were amidated with 2-(phenylethyl)amine.[17] The amidation reaction was monitored by means of IR spectroscopy: the peak at ~1690 cm^{-1} assigned to the stretching mode of the carbonyl group of the carboxylic acid disappeared and shifted to ~1640 cm^{-1} after the modification (Figure S2).[17] The Au core retained its structure during the amidation because the powder XRD pattern (Figure 2) did not change appreciably after the reaction.

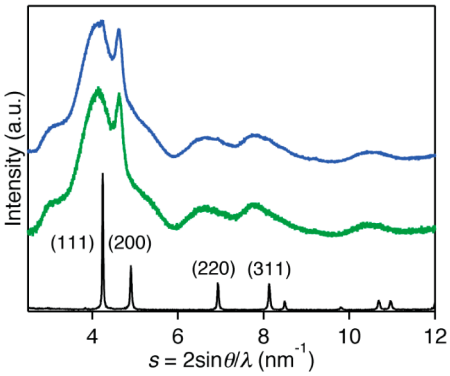

Figure 2. Powder XRD patterns of **1** (green), **2** (blue), and bulk gold (black) recorded under the same experimental setup.

The amidated cluster **2** in $CHCl_3$ (Figure 1b) exhibits similar spectral profile with the filmed sample of **1**. These results lead us to conclude that the NIR absorption bands of **1** and **2** reflect their intrinsic natures.

To determine whether the NIR band is associated with the size or the morphology of the Au core, we examined the structures of Au cores in more detail. The ESI mass spectrum of **1** measured in the negative-ion mode (Figure S3)[17] was dominated by a series of multiply charged anions formed by deprotonation of the carboxylic acid group of the 4-MEBA ligand. The molecular weight (MW) of cluster **1** was determined to be 22.9 kDa. However, because of the limited accuracy of this mass determination, we could not determine the chemical composition unambiguously, as there were several possible candidates, including Au_{73}(4-MEBA)$_{47}$, Au_{74}(4-MEBA)$_{46}$, Au_{75}(4-MEBA)$_{45}$, or Au_{76}(4-MEBA)$_{44}$ (Table 1). To assist in the assignment of the

Table 1. Chemical Compositions of 1 and 2

	cluster **1**		cluster **2**
composition[a]	MW[b] (Da)	weight loss (%)[c]	weight loss (%)[c]
73, 47	22896	37.2	48.1
74, 46	22912	36.4	47.3
75, 45	22928	35.5	46.4
76, 44	22944	34.7	45.5
experiment	22.9×10^3	35.1	45.3

[a]The numbers of Au atoms and thiolate moieties, respectively. [b]Calculated molecular weight for each composition. [c]Calculated weight loss for each composition.

composition, we conducted a thermogravimetric analysis (TGA). The TGA curve (Figure S4)[17] showed that a 35.1% weight loss occurred in the temperature range 200−900 °C, after release of residual water in the range 50−120 °C. These results suggest that the composition of cluster **1** is either Au_{75}(4-MEBA)$_{45}$ or Au_{76}(4-MEBA)$_{44}$. To narrow this down, we conducted TGA of **2**.[17] TGA of **2** showed a weight loss of 45.3% (Figure S5, Table 1),[17] leading us a tentative assignment of the stoichiometry $Au_{76}(SR)_{44}$ to **1** and **2**. Optical spectra of similar-sized clusters, such as $Au_{67}(SR)_{35}$,[18] $Au_{75}(SR)_{40}$,[19] and $Au_{99}(SR)_{42}$[20] show basically featureless exponential-like profiles that are unlike that in Figure 1. $Au_{64}(SR)_{32}$ shows a small peak at 960 nm in addition to those at 400 and 520 nm.[21] However, the relative intensity of the NIR peak is much smaller than those in the UV−vis region in $Au_{64}(SR)_{32}$ in sharp contrast to the case of $Au_{76}(SR)_{44}$ (Figure 1). These comparisons indicate that the cluster size is not a direct cause for the intense NIR absorption.

The strong NIR band is reminiscent of a longitudinal LSP band at ~2300 nm in Au UNRs (diameter ≈ 1.6 nm, length ≈ 20 nm).[10] Thus, another possible reason for the intense NIR absorption of **1** and **2** might be an anisotropic geometric structure of the Au core. Since crystallization trials were unsuccessful, we considered the morphology and atomic packing of **1** and **2** on the basis of powder XRD data (Figure 2). The diffraction patterns cannot be explained by assuming an icosahedral or decahedral motif (Figure S6),[17] but they do resemble patterns for an fcc motif.[22] The most notable feature of Figure 2 is that the diffraction peak for (200) is much sharper than the other peaks, which are broadened as a result of the small crystalline size. This indicates that the Au core has a one-dimensional structure that is elongated along the {100} direction. A simple electron-counting scheme[23] suggests that the formal number of valence electrons in the core of $Au_{76}(SR)_{44}$ is 32. This number does not correspond to any of those expected for an isotropic spherical Au core, such as 8, 18, 20, 34, etc. This consideration also supports a nonspherical structure Au core of **1** and **2**. We attempted to directly image the morphologies by transmission electron microscopy. However, we only observed small (<2 nm) spherical particles that were probably transformed by electron beam irradiation.

An atomic-structure model for the one-dimensional fcc core was developed by simulating the powder XRD pattern. Given that Au-thiolate oligomers are formed on the surface of the Au cores of **1** and **2**, the number of Au atoms in the cores should be in the range 40−50. Here, we limit ourselves to considering three model structures that have an elongated fcc structure and axial symmetry along the {100} direction. The first model is a Au_{49} core consisting of five Au_{13} cuboctahedra with shared (100) facets (Figure 3a). The second model is a Au_{56} core consisting of four Au_{17} truncated octahedra that share (100) facets (Figure 3b). The third model is a Au_{52} core consisting of four Au_{13} cuboctahedra with attached (100) facets (Figure 3c). Figure 3d shows the XRD patterns for these three models structures, simulated by using the Debye formula[17,24] with the assumption that the Au−Au bond length is the same as that in the bulk Au (0%). The polycuboctahedral Au_{49} model (Figure 3a) reproduced the diffraction peak from (200) more closely than did the other models. However, the peak position for (200) was markedly shifted to a smaller s value compared with that of bulk Au (Figure 2). This trend indicates that the lattice spacing of **1** and **2** is significantly expanded in comparison to that of the bulk Au. We next simulated the patterns by expanding the structure along the {100} direction by 1−5% (Figure S7).[17] As shown in Figure 3d, the polycuboctahedral Au_{49} model in which all the Au−Au bonds were expanded by 5% reproduced the experimental powder XRD pattern. Note that another $Au_{76}(SR)_{44}$ model can be constructed by extending the growth sequence rule of $Au_{28}(SR)_{20}$, $Au_{36}(SR)_{24}$, and $Au_{44}(SR)_{28}$ with fcc-based Au cores.[25] This $Au_{76}(SR)_{44}$ model has an Au_{68} core consisting of 14 interpenetrating Au_{13} cuboctahedra, in which the

DOI: 10.1021/jacs.5b03251
J. Am. Chem. Soc. 2015, 137, 7027−7030

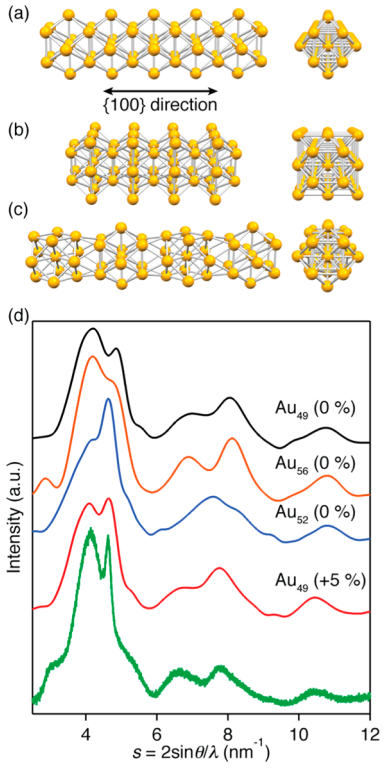

Figure 3. Side and front views of model structures of (a) Au_{49}, (b) Au_{56}, and (c) Au_{52} cores of $Au_{76}(SR)_{44}$ and (d) their simulated XRD patterns. The green plot corresponds to the experimental pattern for **1**.

central atoms of the 14 cuboctahedra are linearly arranged into six edge-sharing tetrahedra (Figure S8a).[17] However, this Au_{68} model could not reproduce the experimental powder XRD pattern (Figure S8b).[17]

Polycuboctahedral Au_{49} core proposed here has several unique structural features as compared to Au UNRs and UNWs stabilized by oleylamine.[10,26−30] First, the diameter of Au_{49} (∼1 nm) is thinner than those of Au UNRs and UNWs (∼1.6 nm) by nearly one-atomic layer. Given that the electron beam irradiation to Au UNWs during TEM observation induces melting and splitting,[27,29,30] it is reasonable that one-dimensional structure of a thinner Au_{49} core of $Au_{76}(SR)_{44}$ could not be imaged by TEM. Second, the Au_{49} core grows along the {100} direction, whereas Au UNWs grow along the {111} direction.[26−30] Finally, the length of the Au_{49} core is precisely defined. These features will provide us a platform for studying how the stabilities and properties of superatomic molecules[31] are affected by the size, bonding mode, and number of constituent superatoms.

What is the origin of the NIR bands of **1** and **2**? It is important to note that the effect of coupling between neighboring clusters upon the NIR bands (Figure 1) is negligibly small. The molar absorption coefficient (ε) of **2** at 1340 nm was determined to be 3×10^5 M^{-1} cm^{-1} (Figure 1b). This ε value is much larger than that for the HOMO−LUMO transition of $Au_{25}(SR)_{18}^-$ (8.8×10^3 M^{-1} cm^{-1}),[32] but is slightly smaller than that for the LSP of $Au_{\sim 500}(SR)_{\sim 120}$ (1.42×10^6 M^{-1} cm^{-1}).[33] This value of ε can be explained within either the framework of an electronic transition[11,16] or a longitudinal mode of LSP[12−15] as follows. First, it has been predicted that linear assemblies of icosahedral Au_{13} units should exhibit a strong absorption in the NIR region as a result of photoexcitation of a free electron in a one-dimensional box.[16] The intense NIR absorbance is explained in terms of the formation of a large dipole in the longitude direction upon photoexcitation.[16] Thus, the large value of ε of **2** can be ascribed to the large electronic-transition moment arising from the one-dimensional structure of **2**. Second, the ε value of **2** is reasonable for LSP if we consider that the number of free electrons is reduced significantly as compared with $Au_{\sim 500}(SR)_{\sim 120}$. Further work is necessary to unravel the nature of the NIR bands of **1** and **2**.

The formation of a one-dimensional structure may result from the slow reduction of the Au precursor ions in the highly basic conditions (pH > 12). A rapid reduction without adjusting the pH value to >12 gave spherical clusters that showed an exponential-like optical absorption spectrum and a brownish color (Figure S9). Similarly, slow reduction of Au ions in the presence of oleylamine was key to the successful synthesis of Au UNWs and UNRs.[10,26−30] It is widely accepted that the complexes of Au(I) and oleylamine serve as growth template and govern the anisotropic growth. Preliminary measurement of time-resolved optical spectra during the synthesis (data not shown) demonstrated that the NIR band was red-shifted discontinuously with time. This result supports that the length of the Au core increases gradually. The slow and anisotropic growth of the Au core may be governed by the oligomeric structures of the Au(I)-SR precursors. Details of the formation process for the cluster will be studied by characterizing isolated intermediates formed during the slow reaction.[26−30,34,35]

In summary, we report the synthesis of $Au_{76}(SR)_{44}$ exhibiting a strong NIR absorption band. The powder XRD pattern of the material was reproduced by assuming the existence of a Au_{49} core consisting of five Au_{13} cuboctahedra sharing their (100) facets.

■ ASSOCIATED CONTENT

Supporting Information

Synthetic details, ESI-MS spectrum, TGA, IR spectra, powder XRD patterns, and XRD pattern simulations. The Supporting Information is available free of charge on the ACS Publications website at DOI: 10.1021/jacs.5b03251.

■ AUTHOR INFORMATION

Corresponding Author

*tsukuda@chem.s.u-tokyo.ac.jp

Notes

The authors declare no competing financial interest.

■ ACKNOWLEDGMENTS

We thank Dr. I. Osaka (JAIST) for his kind trial for ESI-MS measurement. This research was financially supported by the Elements Strategy Initiative for Catalysis & Batteries (ESICB), a Grant-in-Aid for Scientific Research (No. 26248003), and Nanotechnology Platform Program of from the Ministry of Education, Culture, Sports, Science, and Technology (MEXT) of Japan. S.T. is grateful for a JSPS Research Fellowship for Young Scientists.

■ REFERENCES

(1) Kamat, P. V. *J. Phys. Chem. B* **2002**, *106*, 7729.
(2) Murphy, C. J.; Sau, T. K.; Gole, A. M.; Orendorff, C. J.; Gao, J.; Gou, L.; Hunyadi, S. E.; Li, T. *J. Phys. Chem. B* **2005**, *109*, 13857.
(3) Pérez-Juste, J.; Pastoriza-Santos, I.; Liz-Marzán, L. M.; Mulvaney, P. *Coord. Chem. Rev.* **2005**, *249*, 1870.
(4) Alvarez, M. M.; Khoury, J. K.; Schaaff, T. G.; Shafigullin, M. N.; Vezmar, I.; Whetten, R. L. *J. Phys. Chem. B* **1997**, *101*, 3706.

DOI: 10.1021/jacs.5b03251
J. Am. Chem. Soc. 2015, 137, 7027−7030

(5) Hostetler, M. J.; Wingate, J. E.; Zhong, C.-J.; Harris, J. E.; Vachet, R. W.; Clark, M. R.; Londono, J. D.; Green, S. J.; Stokes, J. J.; Wignall, G. D.; Glish, G. L.; Porter, M. D.; Evans, N. D.; Murray, R. W. *Langmuir* **1998**, *14*, 17.
(6) Negishi, Y.; Nakazaki, T.; Malola, S.; Takano, S.; Niihori, Y.; Kurashige, W.; Yamazoe, S.; Tsukuda, T.; Häkkinen, H. *J. Am. Chem. Soc.* **2015**, *137*, 1206.
(7) Jin, R. *Nanoscale* **2010**, *2*, 343.
(8) Maity, P.; Xie, S.; Yamauchi, M.; Tsukuda, T. *Nanoscale* **2012**, *4*, 4027.
(9) Jin, R. *Nanoscale* **2015**, *7*, 1549.
(10) Takahata, R.; Yamazoe, S.; Koyasu, K.; Tsukuda, T. *J. Am. Chem. Soc.* **2014**, *136*, 8489.
(11) Nobusada, K.; Iwasa, T. *J. Phys. Chem. C* **2007**, *111*, 14279.
(12) Guídez, E. B.; Aikens, C. M. *J. Phys. Chem. C* **2013**, *117*, 12325.
(13) Piccini, G. M.; Havenith, R. W. A.; Broer, R.; Stener, M. *J. Phys. Chem. C* **2013**, *117*, 17196.
(14) Burgess, R. W.; Keast, V. J. *J. Phys. Chem. C* **2014**, *118*, 3194.
(15) López-Lozano, X.; Barron, H.; Mottet, C.; Weissker, H.-C. *Phys. Chem. Chem. Phys.* **2014**, *16*, 1820.
(16) Malola, S.; Lehtovaara, L.; Häkkinen, H. *J. Phys. Chem. Lett.* **2014**, *5*, 1329.
(17) See Supporting Information.
(18) Nimmala, P. R.; Yoon, B.; Whetten, R. L.; Landman, U.; Dass, A. *J. Phys. Chem. A* **2013**, *117*, 504.
(19) Balasubramanian, R.; Guo, R.; Mills, A. J.; Murray, R. W. *J. Am. Chem. Soc.* **2005**, *127*, 8126.
(20) Li, G.; Zhen, C.; Jin, R. *J. Am. Chem. Soc.* **2014**, *136*, 3673.
(21) Zeng, C.; Chen, Y.; Li, G.; Jin, R. *Chem. Mater.* **2014**, *26*, 2635.
(22) Cleveland, C. L.; Landman, U.; Schaaff, T. G.; Shafigullin, M. N.; Stephens, P. W.; Whetten, R. L. *Phys. Rev. Lett.* **1997**, *79*, 1873.
(23) Walter, M.; Akola, J.; Lopez−Acevedo, O.; Jadzinsky, P. D.; Calero, G.; Ackerson, C. J.; Whetten, R. L.; Grönbeck, H.; Häkkinen, H. *Proc. Natl. Acad. Sci. U.S.A.* **2008**, *105*, 9157.
(24) Lopez-Acevedo, O.; Akola, J.; Whetten, R. L.; Grönbeck, H.; Häkkinen, H. *J. Phys. Chem. C* **2009**, *113*, 5035.
(25) Zeng, C.; Chen, Y.; Li, G.; Jin, R. *Chem. Commun.* **2014**, *50*, 55.
(26) Halder, A.; Ravishankar, N. *Adv. Mater.* **2007**, *19*, 1854.
(27) Lu, X.; Yavuz, S.; Tuan, H.-Y.; Korgel, B. A.; Xia, Y. *J. Am. Chem. Soc.* **2008**, *130*, 8900.
(28) Hou, Z.; Tsung, X.-K.; Huang, W.; Zhang, X.; Yang, P. *Nano Lett.* **2008**, *8*, 2041.
(29) Pazos-Perez, N.; Baranov, D.; Irsen, S.; Hilgendorff, M.; Liz-Marzán, L. M.; Giersig, M. *Langmuir* **2008**, *24*, 9855.
(30) Feng, H.; Yang, Y.; You, Y.; Li, G.; Guo, J.; Yu, T.; Shen, Z.; Wu, T.; Xing, B. *Chem. Commun.* **2009**, 1984.
(31) Nishigaki, J.; Koyasu, K.; Tsukuda, T. *Chem. Rec.* **2014**, *14*, 897.
(32) Negishi, Y.; Nobusada, K.; Tsukuda, T. *J. Am. Chem. Soc.* **2005**, *127*, 5261−5270.
(33) Kumara, C.; Zuo, X.; Ilavsky, J.; Chapman, K. W.; Cullen, D. A.; Dass, A. *J. Am. Chem. Soc.* **2014**, *136*, 7410.
(34) Yuan, X.; Zhang, B.; Luo, Z.; Yao, Q.; Leong, D. T.; Yan, N.; Xie, J. *Angew. Chem., Int. Ed.* **2014**, *53*, 4623.
(35) Luo, Z.; Nachammai, V.; Zhang, B.; Yan, N.; Leong, D. T.; Jiang, D.; Xie, J. *J. Am. Chem. Soc.* **2014**, *136*, 10577.

DOI: 10.1021/jacs.5b03251
J. Am. Chem. Soc. 2015, 137, 7027−7030